Gate-tunable quantum transport in double-layer graphene

K. Kechedzhi, E. H. Hwang, and S. Das Sarma
Condensed Matter Theory Center, Department of Physics, University of Maryland, College Park, Maryland 20742-4111, USA
(Received 22 August 2012; published 25 October 2012)

We analyze the effect of screening provided by the additional graphene layer in double-layer graphene heterostructures (DLGs) on transport characteristics of DLG devices in the metallic regime. The effect of gate-tunable charge density in the additional layer is twofold: it provides screening of the long-range potential of charged defects in the system, and screens out Coulomb interactions between charge carriers. We find that the efficiency of defect charge screening is strongly dependent on the concentration and location of defects within the DLG. In particular, only a moderate suppression of electron-hole puddles around the Dirac point induced by the high concentration of remote impurities in the silicon oxide substrate could be achieved. A stronger effect is found on the elastic relaxation rate due to charged defects resulting in mobility strongly dependent on the electron density in the additional layer of DLG. We find that the quantum interference correction to the resistivity of graphene is also strongly affected by screening in DLG. In particular, the dephasing rate is strongly suppressed by the additional screening that suppresses the amplitude of electron-electron interaction and reduces the diffusion time that electrons spend in proximity of each other. The latter effect, combined with screening of elastic relaxation rates, results in a peculiar gate-tunable weak-localization magnetoresistance and quantum correction to resistivity. We propose suitable experiments to test our theory and discuss the possible relevance of our results to existing data.

DOI: 10.1103/PhysRevB.86.165442 PACS number(s): 72.80.Vp, 72.15.Rn, 71.10.Ay, 73.21.−b

I. INTRODUCTION

Gate-tunable Anderson localization of Dirac electrons is inaccessible in standard field-effect heterostructures due to the strong disorder-induced inhomogeneity of the local doping level (electron-hole puddles)[1–6] ubiquitous in the materials that show Dirac-type low-energy spectrum, such as graphene[7] or topological insulator surfaces.[8] Basically, the low-density localization behavior of graphene is inaccessible experimentally because the Dirac point itself is inaccessible due to the formation of electron-hole puddles around the charge neutrality point. However, very recently, a novel double-layer graphene (DLG) heterostructure containing two graphene layers separated by an insulator allowed using additional screening effect of the second graphene layer to access a metal-insulator transition regime. Anomalously large resistance $\rho \gg h/(4e^2)$, in combination with insulating temperature dependence, was observed in these experiments suggestive of a metal-insulator transition (MIT).[9] The physical nature of this behavior is currently a topic of a debate.[9,10] In particular, whether the transport data of Ref. 9 represent an effective low-density high-temperature semiclassical resistivity[10] or a low-temperature strong Anderson localization crossover behavior[9] is unclear at this stage.

On the one hand, suppressing inhomogeneity allows access to the low-density regime $k_F\ell \lesssim 1$ in which Anderson physics is expected to dominate (here, k_F is the Fermi wave vector and ℓ is the mean-free path). In this regime, quantum interference of the two flavors (due to two valleys) of chiral Dirac charge carriers in graphene may result in the insulating behavior in the case of sufficient mixing of the flavors by atomic-scale disorder.[9,11,12] On the other hand, the experiments of Ref. 9 were restricted to a fairly high-temperature regime (10–100 K) where quantum interference effects may be suppressed due to short phase-breaking length. The observed MIT is also in contrast with more recent transport measurements on ultrahigh-quality suspended devices[13] in which an extremely low-density inhomogeneity is achieved, $\delta n \sim 10^8$ cm^{-2}; nevertheless, no MIT is detected (see also more recent experiment Ref. 14). Moreover, an Anderson insulator would be characterized by the resistivity growing exponentially with decreasing temperature, whereas the data[9] demonstrate only a roughly power-law growth. Insulating power-law temperature dependence (resistivity growing with decreasing temperature) is not unusual near charge neutrality in graphene (see Fig. 2 in Ref. 9, and measurements on other low[15,16] and high[13,17] mobility samples). This behavior is explained by the combined effect of temperature-dependent screening[18] thermal excitation of electrons from the valence band and thermally activated hopping of electrons over the potential barriers between electron-hole puddles.[19] Nevertheless, very high values of resistance reported in Ref. 9, $\rho \gg h/(4e^2)$, suggest a novel behavior in this system possibly associated with MIT. However, an alternative explanation for the observed behavior was recently suggested,[10,19] in which case the anomalous resistance is explained by a Boltzmann transport effect combined with strong suppression of inhomogeneity in DLG.[10,19] The latter work is phenomenological and relies on the assumptions of the quasiclassical transport formalism and the phase-breaking length being shorter than the elastic-scattering length. Therefore, a more detailed analysis of quantum effects is required to justify the applicability of the latter approach. One way to make progress in the understanding of the observed behavior of the resistivity in these devices is to analyze the metallic regime where perturbation expansion in disorder strength may be applied. Such theoretical analysis of the quantum interference effect in the higher-density weak-localization regime of the DLG system, which must be a precursor to any low-density strong-localization crossover phenomenon, is one of the main goals of our work.

In this paper, we consider the effect of gate-tunable screening provided by the additional layer in DLGs on

 ©2012 American Physical Society

transport characteristics of these devices. Screening affects both the potential of charged defects and Coulomb interactions of charge carriers. Taking into account both effects, we analyze the classical and quantum parts of the resistivity of graphene in DLG geometry in the metallic regime $k_F \ell \gg 1$. We consider only the low-temperature regime such that elastic scattering by the disorder limits the transport characteristics, and all inelastic scattering effects may be included perturbatively.

We outline the results of the following analysis: (i) We develop a framework describing the screening effect of the two graphene layers in DLG on the Coulomb potential of charged defects in the DLG heterostructure. (ii) We generalize the self-consistent theory of disorder-induced electron density fluctuations at neutrality point of graphene[1] (electron-hole puddles) and use it to estimate the screening effect of DLG on the amplitude of the electron density fluctuations. (iii) We analyze the effect of screening in DLG on the elastic-scattering rate due to charged defects that determine the extent of gate tunability of mobility in DLG. (iv) We analyze the effect of the screening in DLG on the dephasing rate due to inelastic electron-electron collisions. (v) We analyze the combined effect of screening on the weak-localization correction to the resistivity. (vi) We predict a peculiar gate-tunable magnetoresistance in the high-quality DLG structures with mixed elastic-scattering mechanisms.

This work is limited to the perturbative metallic regime and can not make any definitive conclusions about the regime of the low density studied in the experiments of Ref. 9. However, the theoretical framework developed in the following provides a basis for analysis of more detailed gate-tunable quantum transport measurements which would allow characterization of various microscopic scattering mechanisms that determine the behavior of the system in the low-density regime. In particular, we believe that it is imperative that we understand the high-density metallic regime of the DLG transport in some depth before trying to understand the low-density crossover MIT regime since a systematic perturbative theory is available in the higher-density regime, whereas the low-density regime is inaccessible to analytical theory. We hope that our work would motivate experimental work focusing on the metallic regime of DLG in order to investigate the conceptually important question of Anderson localization and metal-insulator transition in graphene.

We consider a DLG consisting of two layers of graphene, "studied" and "control" (see Fig. 1), which are used for resistivity measurements and to provide the additional screening effect, respectively. The two layers are separated by a thin layer, $d \gtrsim 4$ nm, of insulating hexagonal boron nitride (hBN) that is thick enough to suppress direct tunneling between the layers. The whole structure is separated by a thick layer, $d_0 \sim 20$ nm, of hBN from the standard SiO_2/Si substrate. The combination of the top and bottom gates in this heterostructure allows independent "control" of the electron densities n_c and n_s in the "control" and "studied" layers, respectively. This setup is motivated by the design of heterostructures in Ref. 9. We assume that the mobility of the studied layer is limited by elastic scattering of charged impurities in accordance with the data.[9]

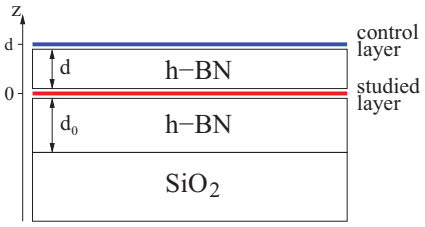

FIG. 1. (Color online) A schematic of a typical double-layer graphene heterostructure used in Ref. 9. Top (blue) and bottom (red) layers correspond to the "control" and "studied" layers, respectively, with typical values of $d = 4$ nm and $d_0 = 20$ nm considered in the text.

The additional screening effect of the control layer is expected to suppress the electron-hole puddles in the studied layer. We find that the effectiveness of the control layer screening strongly depends on the position of impurities in the DLG. It is efficient for the relatively small concentration of charged defects on top of the control layer, whereas it leads to only a moderate suppression of the inhomogeneity induced by charges in close proximity of the studied layer and by the remote charged defects in SiO_2 substrate. The latter inefficiency stems from the very high densities of charged defects in the SiO_2 substrate $n_i \gtrsim 10^{12}$ cm^{-2} that would require screening charge density in the control layer several times n_i, which is beyond the experimentally accessible range. Moreover, the nonlinear screening effects in the electron-hole puddle regime in the studied layer work against the screening effect of the control layer making the screening less efficient. The situation is slightly different in the case of elastic relaxation rate due to charged defects. The screening by control layer is more efficient in this case and leads to the suppression of the classical part of the resistivity near the Dirac point of the studied layer. The resulting behavior of the resistivity as a function of the density in the control layer is a result of a competition of the suppression of electron-hole puddles that increases the resistivity and suppression of the elastic relaxation rate that decreases the resistivity.

In the following, we also demonstrate that the ratio of momentum relaxation rate to the transport rate varies substantially with the distance between graphene and charged defects. Therefore, measurement of the two elastic relaxation rates can be used to determine the location of charged defects limiting the mobility in DLG. The transport scattering rate can be extracted from Boltzmann resistivity. The momentum relaxation rate characterizes the broadening of single-particle states and can be extracted from the decay of Shubnikov–de Haas oscillations. A similar technique[20] has been successfully applied to the analysis of the standard graphene-based field-effect transistors.[21] Since our work establishes that the inhomogeneous puddles induced by the distant charged impurities in SiO_2 can be suppressed only partially by the control layer screening, it is important to know where the dominant charged impurities reside and the measurement of the single-particle momentum relaxation (sometimes also called the quantum scattering) time could help locate the charged impurities in the DLG system.

Very high values of the mobility of the studied layer encapsulated in hBN that is tunable in the range 50–120 $\times$ 10^3 cm^2 V^{-1} s^{-1} with the screening density in control layer

n_c indicate the dominant role of the charged defects in the elastic scattering in this system. Furthermore, the very high value of the observed[9] maximum of the gate-tunable mobility suggests a weak effect of neutral (immune to screening) elastic-scattering mechanisms that break locally the lattice symmetry of graphene. Therefore, these DLGs may demonstrate quantum interference behavior distinct from that observed in typical graphene flakes[22–31] where strong lattice-symmetry-breaking disorder determines predominantly weak-localization behavior. This is especially so at relatively low densities n_s at which the effect of trigonal warping of the Fermi line[32] can be neglected.

Two identical carbon atoms in the unit cell of graphene give rise to two degenerate flavors (valleys) of chiral Dirac charge carriers in its electronic spectrum confined to the vicinities of the two inequivalent corners of the hexagonal Brillouin zone. Quantum interference of two independent flavors of Dirac quasiparticles is associated with weak-antilocalization behavior.[32,33] The latter is, however, protected only by the symmetry between the two sublattices in graphene, which can be easily broken by impurities. Therefore, quantum interference in graphene is very sensitive to the presence of elastic-scattering mechanisms that break lattice symmetry. Generic time-inversion-symmetric disorder in graphene can be categorized into three types according to their effect on quantum interference: (i) potential of the charged defects that do not break lattice symmetry; (ii) smooth random vector potential disorder that breaks the symmetry between the two carbon atoms in the unit cell of graphene (intravalley disorder); (iii) atomic-scale disorder that breaks lattice symmetry and causes mixing of the two valleys (intervalley disorder). Random vector potential disorder leads to suppression of the weak-antilocalization effect, whereas the intervalley scattering restores the weak-localization behavior typical for two-dimensional electron gas. In the case of high-quality DLG heterostructures with very weak lattice-symmetry-breaking scattering, the weak-antilocalization effect of Dirac electrons plays an important role.

Additional screening in DLG affects only the scattering rate due to charged defects in graphene and therefore changes the relative strength of intravalley and intervalley defects with respect to the strength of potential scatterers. This results in the dependence of quantum correction on the electron density in the control layer n_c. In particular, an interesting possibility arises that the intervalley elastic scattering, while being unimportant in determining the semiclassical Boltzmann resistivity, becomes important in determining the tuning of the quantum interference correction from antilocalization to localization.

In a wide temperature range, quantum interference is limited by decoherence rate due to inelastic electron-electron collisions. The latter is strongly affected by the screening effect in DLG for two reasons: due to suppression of the Coulomb interaction between charge carriers, and due to enhancement of the diffusion coefficient that reduces the time electrons spend in proximity of each other where interaction is the strongest. The combination of these two effects results in strong variation of the decoherence rate with the screening density. This gives rise to a peculiar gate-tunable quantum correction to the resistivity of graphene in DLG devices which may change sign depending on the screening density in the control layer, especially at higher temperatures. It should be emphasized that this gate-tunable quantum correction to the Boltzmann resistivity is manifest only when the phase-breaking length is much larger than the elastic mean-free path, i.e., at lower temperatures, so that the quantum interference is operational. Since our theory treats the quantum correction perturbatively, it applies only in the metallic regime at densities well above the crossover to strong Anderson localization.

The most striking consequence of the gate-tunable quantum correction can be observed in the intermediate density regime in which the transport in the studied layer is metallic, $k_F\ell \gg 1$, whence the Fermi energy is low enough so that the trigonal warping effect is negligible. The quantum correction in this case is strongly dependent on the electron density in the control layer. At sufficiently strong dephasing rate (sufficiently high temperature), this results in a gate-tunable crossover from weak-antilocalization-type magnetoresistance to weak-localization type. A similar crossover that was temperature driven was demonstrated in graphene previously;[26,30] our work demonstrates a similar tunability with the gate voltage in DLG systems.

The quantum part of the resistivity also includes the Altshuler-Aronov correction to the conductivity due to the electron-electron interactions[34,35] which typically has the sign enhancing the localization effect and is expected to be suppressed by the additional screening effect that typically reduces the interaction strength. This does not have any effect on low-field magnetoresistance, which allows us to study the quantum interference (weak-localization) correction separately.

The paper is organized as follows. In Sec. II, we analyze the effect of control layer screening on Coulomb potentials of the charged defects. Sections III and IV discuss classical and quantum parts of the resistivity, respectively. We provide a discussion of the relevance of our work to experiments, particularly the data of Ref. 9, where the DLG system was studied experimentally in Sec. V. We conclude in Sec. VI.

II. SCREENING EFFECT OF THE "CONTROL" LAYER

A. Linear screening in DLG

We start with a linear screening model for DLG heterostructure. For simplicity, we assume that a density n_i of charged defects is located in a plane a distance z from the "studied" layer (at $z = 0$), which can be both above $z > 0$ and below $z < 0$ it. The "control" layer is located at a distance d above the studied layer (see Fig. 1).

We include both intralayer and interlayer Coulomb interactions between electrons in DLG described by a symmetric matrix $U_{\ell\ell'}$ with diagonal $U_{11} = U_{22} = \upsilon_q$, and off-diagonal elements $U_{12} = U_{21} = \upsilon_q e^{-qd}$ with $\upsilon_q = 2\pi e^2/q$ being the two-dimensional (2D) Fourier transform of the Coulomb potential. Here, $\ell,\ell' = 1,2$ correspond to the studied and control layers, respectively. We calculate the interaction energy of an impurity charge Z_1 and a conduction electron charge Z_2 in the studied layer in the presence of the screening effect of electron gases in both studied and control layers. This can be found using linked cluster expansion of the thermodynamic

potential[36] of the DLG. In the resulting infinite series, we keep only the term proportional to the product of the two charges that represents the linear screening of the interaction potential,

$$\Delta\Omega(\mathbf{R_1}-\mathbf{R_2}) = Z_1 Z_2 \int \frac{d\mathbf{q}}{(2\pi)^2}\frac{\upsilon_q e^{-q|z|}}{\varepsilon_z(\mathbf{q})} e^{i\mathbf{q}\cdot(\mathbf{R_1}-\mathbf{R_2})}, \qquad (1)$$

where q and $\mathbf{R}_i$ are 2D wave vector and position vector, respectively, and $Z_1 Z_2 e^{-q|z|}\upsilon_q$ is the Fourier transform of the bare Coulomb interaction between the charges Z_1 and Z_2. For electrons, we can put $Z_1 = Z_2 = 1$. In Eq. (1), we introduced a dielectric function

$$\frac{1}{\varepsilon_z(\mathbf{q})} = 1 - \frac{e^{q|z|}\upsilon_q}{2}\sum_{\ell\ell'} D_{\ell\ell'}(q)\chi_{\ell\ell'}(\mathbf{q}), \qquad (2)$$

where the matrix $D_{\ell\ell'}(q)$ takes into account the dependence of Coulomb interaction energy on the spatial separation between the charges in the z direction:

$$D_{\ell\ell'}(q) = \begin{bmatrix} 2e^{-q|z|} & e^{-q|d-z|}+e^{-q(d+|z|)} \\ e^{-q|d-z|}+e^{-q(d+|z|)} & 2e^{-qd} \end{bmatrix}.$$

Here, $\chi_{\ell\ell'} = \langle T_\tau \rho_\ell(\mathbf{q},\tau)\rho_{\ell'}(-\mathbf{q},0)\rangle$ is the density-density correlator which is a matrix in the layer index $\ell = 1,2$, including both intralayer and interlayer terms. The density-density correlator is renormalized by the Coulomb interaction matrix, which is given by an infinite perturbative series.[37] Within the random phase approximation, the result of the resummation of the perturbation series satisfies a matrix Dyson equation[38,39]

$$\hat{\chi}^{-1} = (\hat{\chi}^{(0)})^{-1} + \hat{U}, \qquad (3)$$

where $\hat{\chi}^{(0)}$ is the diagonal matrix of free-particle polarization operators in the two graphene layers. Solving the Dyson equation (3), we arrive at the dielectric function in the form

$$\frac{1}{\varepsilon_z(\mathbf{q})} = \frac{1+\upsilon_q\chi_{22}^{(0)}(1-e^{-qx})}{d(q)},$$
$$d(q) \equiv \left(1+\upsilon_q\chi_{11}^{(0)}\right)\left(1+\upsilon_q\chi_{22}^{(0)}\right) - \upsilon_q^2 e^{-2qd}\chi_{11}^{(0)}\chi_{22}^{(0)}, \qquad (4)$$

where $x \equiv |z-d|-|z|+d$. The dielectric function (4) demonstrates a strong dependence on both the impurity location z and the interlayer distance d, and in the limit $d\to\infty$ approaches the monolayer form $1/\varepsilon(q) = 1/(1+\upsilon_q\chi_{11}^{(0)})$.

Static screening is described by the zero-frequency limit of the free-particle polarization operator[40,41]

$$\chi_{ii}^{(0)} = g\nu_i\left[\theta\left(2k_F^{(i)}-q\right)+\theta\left(q-2k_F^{(i)}\right)\mathcal{F}(q)\right],$$
$$\mathcal{F}(q) = 1+\frac{\pi q}{8k_F^{(i)}} - \frac{1}{2}\sqrt{1-\frac{4\left(k_F^{(i)}\right)^2}{q^2}} - \frac{q}{4k_F^{(i)}}\arcsin\frac{2k_F^{(i)}}{q},$$

where $\theta(t)$ stands for Heaviside step function, $g = 4$ stands for spin and valley degeneracy combined, $k_F^{(i)}$ and ν_i stand for the Fermi wave vector and the density of states per spin per valley at the Fermi level in the ith layer, respectively.

B. Nonlinear screening in the electron-hole puddle regime

We estimate the effect of screening by the control layer on the density inhomogeneity in the studied layer using the simple self-consistent approach that had shown good agreement with more detailed Thomas-Fermi-Dirac numerical calculations in the case of monolayer graphene.[1,42,43] This estimate is based on the approximate relation $\langle E_F^2\rangle \approx \langle V^2\rangle$, where the amplitude of the fluctuation of the local Fermi energy is equated to the local fluctuation in the potential energy of electrons, which reflects the local electrochemical equilibrium condition. We further assume that the local Fermi level is given by the free-particle form $E_F = \hbar\upsilon_F k_F^{(1)} = \hbar\upsilon_F\sqrt{\pi n_s}$, where υ_F and n_s stand for the Fermi velocity of Dirac electrons and local density, respectively. We also assume that the screening of impurity potential can be taken into account within linear approximation (4). We then end up with a self-consistent equation for the typical density fluctuation n^*. The solution of this self-consistent problem is plotted in Fig. 2 as a function of the control layer density n_c. The discrepancy between the solid black line in Fig. 2(a) as $n_c\to 0$ and the root-mean-square density in monolayer without the screening layer under the same conditions, dashed line, originates from the screening by interband transitions in the control layer at neutrality. The above analysis neglects nonlinear screening effects in the control layer and therefore the saturation in the realistic DLG device may be at a slightly different value. Nevertheless, Fig. 2 and the comparison to the monolayer case give a reasonable estimate of the suppression of the density inhomogeneity by screening.

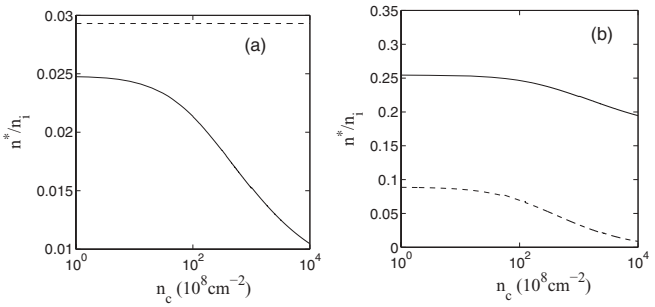

FIG. 2. The result of the self-consistent density calculation in the studied layer as a function of the density in the control layer n_c for a DLG with $d = 4$ nm (see Sec. II B for details). (a) Solid line corresponds to $z = -20$ nm, $n_i = 10^{12}$ cm^{-2}. The horizontal dashed line corresponds to the result of the self-consistent density calculation for isolated monolayer graphene encapsulated in hBN with the same parameters as the solid line. (b) Solid and dashed lines correspond to $z = 1$ and 5 nm, respectively, with the impurity density $n_i = 10^{11}$ cm^{-2}.

C. Location of impurities in DLG

Effectiveness of screening by the control layer is strongly dependent on the location of impurities (z) which can accumulate in three possible areas: Relatively small densities of charged defects $n_i \sim 10^{10}$–10^{11} cm^{-2} can be located at hBN-graphene interfaces[44] and on top of the control layer which can be exposed to air in realistic DLGs. A much larger concentration of charged impurities $n_i \sim 10^{12}$ cm^{-2} is expected to accumulate at the surface of SiO_2 substrate that is separated from the studied layer by $d_0 \sim 20$ nm of hBN (see Fig. 1). These defects do not play an important role in transport in the high-density regime $k_F|z| \gtrsim 1$ due to the exponential factors in Eqs. (1) and (4). However, they

dominate transport and density inhomogeneity at very low densities where $k_F|z| \lesssim 1$ and hence the long-range nature of the Coulomb disorder becomes important at low densities near the Dirac point.

The additional screening effect in DLG is the strongest for impurities located on top of the control layer for which the inhomogeneity varies by an order of magnitude [dashed line in Fig. 2(b)]. However, the screening is substantially less efficient for the impurities located in close vicinity of the studied layer and for the high concentration of impurities in SiO_2 substrate [see the solid line in Fig. 2(b)].

Note that our estimate of the density inhomogeneity relies on the assumption that locally electron density resembles quasiparticles in clean graphene. This is unjustified in the case of strong disorder for which $k_F\ell \sim 1$ (see Secs. III A and III B).

III. ELASTIC RELAXATION RATE AND BOLTZMANN RESISTIVITY

A. Transport relaxation rate due to charged defects

Additional screening in DLG leads to a substantial suppression of the transport scattering rate, which in Born approximation reads as

$$\frac{1}{\tau_{\rm tr}^C} = \frac{2\pi}{\hbar} n_i \sum_{\mathbf{p}'} (1-\cos\varphi) |\langle \mathbf{p}'|V|\mathbf{p}\rangle|^2 \delta(\epsilon_{\mathbf{p}} - \epsilon_{\mathbf{p}'}), \qquad (5)$$

where φ and $q \equiv |\mathbf{p}-\mathbf{p}'| = 2k_F|\sin\frac{\varphi}{2}|$ are the scattering angle and momentum of electrons on the Fermi surface in the studied layer, and $|\langle \mathbf{p}'|V|\mathbf{p}\rangle|^2 = \frac{1}{2}(1+\cos\varphi)|\frac{v_q}{\varepsilon(q)}|^2 e^{-2q|z|}$ is the matrix element of the Coulomb potential of a defect in graphene. Figure 3 shows the variation of the transport mean-free path approximated by Eq. (5) within experimentally accessible densities in the control layer 10^9 cm$^{-2} \lesssim n_c \lesssim 10^{12}$ cm^{-2}.

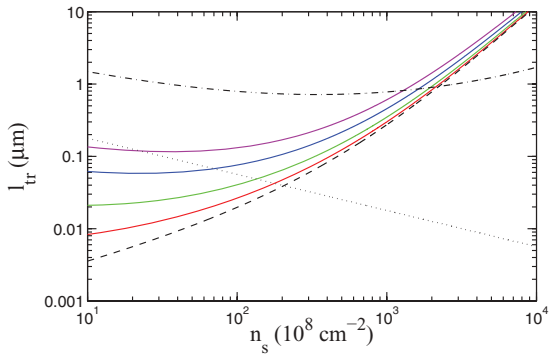

FIG. 3. (Color online) Transport scattering length in the studied layer. Solid lines from bottom to top (red, green, blue, and magenta) correspond to $n_c = 10^9$, 10^{10}, 10^{11}, and 10^{12} cm^{-2}, with $z = -20$ nm, $n_i = 10^{12}$ cm^{-2}. Dashed line corresponds to isolated monolayer graphene with the same parameters. For comparison, the effect of a relatively small concentration of charged defects, $n_i = 10^{11}$ cm^{-2} near the "studied" layer $z = -1$ nm is shown as dashed-dotted line. The dotted line corresponds to $k_F\ell_{\rm tr} = 1$ where quantum and classical parts of the conductivity are of the same order.

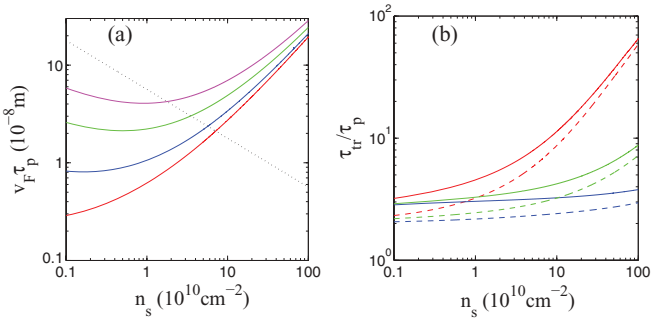

FIG. 4. (Color online) (a) Momentum relaxation rate as a function of the density in the studied layer $n_i = 10^{12}$ cm^{-2}, $z = -20$ nm. Solid lines from bottom to top (red, blue, green, and magenta) correspond to $n_c = 10^9$, 10^{10}, 10^{11}, and 10^{12} cm^{-2}, respectively. Dotted line corresponds to $k_F\ell = 1$ where Born approximation becomes insufficient. (b) Ratio of the transport and momentum relaxation times. Solid lines from bottom to top (blue, green, and red) correspond to ($n_i = 10^{11}$ cm^{-2}, $z = 1$ nm), ($n_i = 10^{11}$ cm^{-2}, $z = 5$ nm), and ($n_i = 10^{12}$ cm^{-2}, $z = -20$ nm), respectively, with $n_c = 10^{12}$ cm^{-2}. Dashed lines correspond to the same parameters with $n_c = 10^8$ cm^{-2}.

B. Momentum relaxation rate: Location of impurities

Different spatial configurations of impurities within DLG may be distinguished experimentally by analyzing the ratio of the momentum relaxation rate to the transport scattering rate. These ratios are substantially different in the cases of scattering on long-range potential of remote and nearby impurities. The transport rate, Eq. (5), is mostly determined by backscattering with large momentum transfer, and therefore decays quickly with the distance z between the charged defects and the studied layer. The momentum relaxation rate, given by,

$$\frac{1}{\tau_p} = \frac{2\pi}{\hbar} n_i \sum_{\mathbf{p}'} |\langle \mathbf{p}'|V|\mathbf{p}\rangle|^2 \delta(\epsilon_{\mathbf{p}} - \epsilon_{\mathbf{p}'}), \qquad (6)$$

includes forward scattering with small momentum transfer, which is only weakly dependent on z [see Fig. 4(a)]. The ratio of the momentum relaxation rate to the transport rate is shown in Fig. 4(b) for the three different locations of impurities considered in Sec. II C. Note that the Born approximation used in Eq. (6) is insufficient when $k_F\ell_p \sim 1$, $\ell_p \equiv v_F\tau_p$ [shown as dotted line in Fig. 6(a)] and further corrections to the elastic relaxation rate have to be included. In the case of remote impurities in SiO_2, there is a peculiar regime where $k_F\ell_p \sim 1$ and the Born approximation is insufficient, yet $k_F\ell_{\rm tr} \gg 1$ which suggests diffusive transport. Note, however, that the perturbative analysis presented here is quantitatively correct only when $k_F\ell_p \gg 1$.

C. Boltzmann resistivity

Suppression of the relaxation rate is reflected in the Boltzmann resistivity $\rho(n_s,n_c) = (\frac{2e^2}{h}k_F\ell_{\rm tr})^{-1}$ shown in Fig. 5(a). It is the strongest near the neutrality point in the studied layer in which case both $n_s \ll n_c$ and $n_s \ll \frac{1}{\pi z^2}$ so that the high concentration of defects in the SiO_2 substrate dominates the transport properties. In the formal limit $2k_F^{(1)} = 2\sqrt{\pi n_s} \ll \kappa_2 = 8\pi e^2 \nu_c$ (κ_2 is the Thomas-Fermi screening wave vector in the control layer), the charged impurity potential becomes

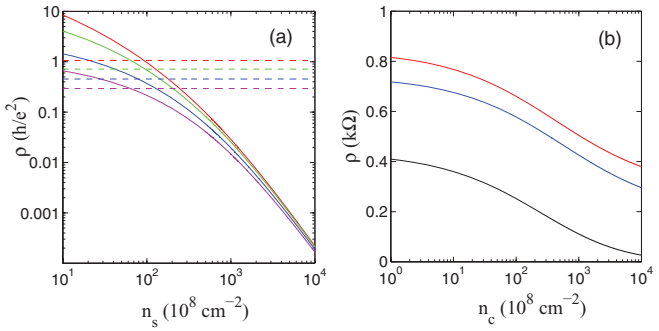

FIG. 5. (Color online) Resistivity of the studied layer $\rho(n_s,n_c)$. (a) Solid lines from top to bottom (red, green, blue, and magenta) correspond to $n_c = 10^9$, 10^{10}, 10^{11}, and 10^{12} cm^{-2}, respectively, with $n_{\rm imp} = 10^{12}$ cm^{-2}, $z = -20$ nm, $d = 4$ nm. Dashed lines correspond to inhomogeneity-induced maximum resistivity with the same parameters from top to bottom. (b) Resistivity at intermediate density $n_s = 10^{11}$ cm^{-2}. Top (red) line corresponds to $n_{\rm imp} = 10^{12}$ cm^{-2}, $z = -20$ nm, bottom (black) and middle (blue) lines correspond to $n_{\rm imp} = 10^{11}$ cm^{-2} and $z = 5$ and 1 nm, respectively.

effectively short ranged, which leads to the resistivity independent of the density n_s,

$$\rho_{\max}(n_c) = \frac{\pi}{16}\left(\frac{h}{2e^2}\right)\frac{n_i}{n_c}(1+4\sqrt{\pi n_c}\alpha x)^2, \qquad (7)$$

where $x = (|z-d| - |z| + d)$. This strong screening limiting resistivity, however, is unlikely to be reached, since within the metallic regime and accessible densities, $k_F^{(1)}/\kappa_2$ is of the order of unity. Moreover, the value of the resistivity at low densities n_s is affected by the doping inhomogeneity. The resistivity maximum in the presence of density inhomogeneity (electron-hole puddles) can be estimated[2,45] using the effective medium theory,[46] which allows averaging of the resistivity of a system split into regions with random values of resistance characterized by a distribution $P[\rho(n)]$. The averaged resistance, $\rho_{\rm EMT}$, in this case is given by the solution of a self-consistent effective medium equation

$$\int dn\, P[n]\frac{\rho(n)-\rho_{\rm EMT}}{\rho(n)+\rho_{\rm EMT}} = 0. \qquad (8)$$

We approximate the distribution of the density fluctuations by a Gaussian with zero average and variance given by $n_{\rm rms} = \langle V^4\rangle$, which compares well with full Thomas-Fermi-Dirac approach[43] in the case of disordered monolayer graphene. The results are shown in Fig. 5(a) as dashed lines. Note, however, that due to the relatively weak doping inhomogeneity induced by the remote impurities in SiO_2, the value of the metallicity parameters $2 \lesssim k_F(n_{\rm rms})\ell_{\rm tr} \lesssim 4$ and $k_F\ell_p \sim 1$ indicate that quantum corrections could be important in this low-density regime. However, the long-range character of the disorder potential makes quantitative analysis of quantum interference difficult[11,47,48] in this regime.

At higher density n_s, the random inhomogeneity can be neglected and transport is metallic, therefore, the linear screening model and the Boltzmann resistivity provide an accurate description of the system. At even higher densities $n_s\pi z^2 \gtrsim 1$, the exponential factors in Eqs. (4) and (5) lead to the strong suppression of the effect of remote impurities in SiO_2. As a result, charged defects in the vicinity of graphene layer and neutral scatterers determine the resistivity. Finally, at the very high density $k_F d \gtrsim 1$, the typical monolayer behavior of the resistivity is restored [see Fig. 5(a)].

D. Intermediate density regime

There exists a regime of densities n_s where Eqs. (4) and (5) provide a quantitatively accurate description of the dependence of the elastic relaxation rate on both densities n_s and n_c. Formally, the constraints defining this regime are as follows: (i) The effect of the density inhomogeneity on the resistivity is negligible, $\sqrt{\overline{(n_s-\overline{n_s})^2}} \ll \overline{n_s}$, where $\overline{O}$ stands for spatial average of O. (ii) Transport in the studied layer is metallic $n_s \gg \frac{1}{\pi\ell_p^2}$. In addition, we assume (iii) that the density in the studied layer is sufficiently small, $n_s \ll n_c$, so that the resistivity changes substantially with changing n_c. Here, n_c is limited by the experimentally accessible density range $n_c \lesssim 5\times 10^{12}$ cm^{-2}. (iv) The trigonal warping of the Fermi line has a negligible effect on weak-localization corrections[32] $\tau_w^{-1}/\tau^{-1} = 2(\pi\mu\hbar\tau n_s)^2 \ll 1$, with $\mu \equiv \frac{v_F a}{4}$ and $a \approx 1.42$ Å is the distance between the nearest neighbors in the hexagonal lattice of graphene. The latter constraint simplifies the analysis of characteristics of various scattering mechanisms that determine the quantum transport in the system. (v) Scattering due to Coulomb defects remains dominant $k_F z \lesssim 1$. Throughout the text, we refer to the range of densities n_s where all constraints (i)–(v) are satisfied as the "intermediate density regime."

The intermediate density regime can be used for a quantitative analysis of both Boltzmann and weak-localization contributions to the resistivity. The effect of screening electron density n_c in the control layer on the resistivity is illustrated in Fig. 5(b). The effect of n_c on the weak-localization correction in the DLG in the intermediate density regime is discussed below.

IV. QUANTUM CORRECTION

We generalize the perturbative theory of weak localization in graphene[32,49] to the DLG heterostructure in the intermediate density regime defined in Sec. III D above.

A. Perturbative theory of weak localization

We briefly review the theory of weak-localization correction to the resistivity of graphene. Weak localization originates from the interference contribution to the probability to scatter backwards. The latter is given by the modulus square of the sum of the quantum mechanical amplitudes A_i associated with each possible backscattered trajectory $P \sim |\sum A_i|^2$. This contains the classical part $P_{cl} \sim \sum |A_i|^2$ and the quantum interference contribution $\delta P \sim \sum A_i A_j^*$. The latter vanishes for generic trajectories. However, in case A_j^* is a time-reversal image of A_i, which is possible for loop-shaped self-intersecting trajectories, the phase factors cancel exactly, $\delta P \sim \sum' |A_i|^2$. Therefore, the average contribution of this special type of trajectory to the backscattering probability is nonzero. δP for a given self-intersecting trajectory is proportional to the ratio of the width of the trajectory $v_F\lambda\, dt$ to the 2D volume Dt that can be spanned by diffusion

during time t. The resulting correction to the conductivity $\delta\sigma \sim \int \lambda v_F dt/(Dt) \sim \ln \tau_\varphi/\tau$ is proportional to the log of the ratio of the travel times along the longest τ_φ and the shortest τ trajectories and is typically of the order of the conductance quantum. The longest trajectories τ_φ that limit the extent of quantum interference are given by either the system size or by phase-breaking effects.

Two degenerate flavors (two valleys) of chiral Dirac fermions in graphene are characterized by an isospin degree of freedom that has a fixed projection on the direction of momentum. Therefore, backscattering of chiral charge carriers is accompanied by the reversal of isospin which gives rise to an additional phase difference πN between the two images of a looped backscattered trajectory, where N is the winding number of the trajectory. The interference contribution to conductivity in this case acquires an additional minus sign, which results in antilocalization[33] effect in contrast to the usual weak localization in 2D.[50] In realistic devices, the vector potential (intravalley) disorder, characterized by a phenomenological rate τ_z^{-1}, breaks the symmetry between the two sublattices of graphene and therefore suppresses the antilocalization effect. Atomic-scale disorder, characterized by τ_{iv}^{-1}, scatters electrons between different valleys and therefore restores the localization sign of the interference correction. Quantitatively, this effect is described by a perturbation expansion in $k_F\ell \gg 1$, which results in the conductivity correction[32]

$$\delta\sigma = -\frac{e^2}{\pi h}\left[\ln\left(1+2\frac{\tau_\varphi}{\tau_{iv}}\right) - 2\ln\frac{\frac{\tau_\varphi}{\tau_{\rm tr}}}{1+\frac{\tau_\varphi}{\tau_{iv}}+\frac{\tau_\varphi}{\tau_z}}\right]. \quad (9)$$

Here, the first term on the left-hand side describes intervalley interference sensitive only to the ratio $\frac{\tau_\varphi}{\tau_{iv}}$; the second term describes the intravalley interference which is also sensitive to smooth intravalley scattering rate τ_z^{-1} due to the vector potential disorder and the total transport scattering rate $\frac{1}{\tau_{\rm tr}} \approx \frac{1}{\tau_{\rm tr}^C}$. The left-hand side in the latter equation, given by Eq. (5), is obtained modeling charged defects by a Gaussian disorder with a finite range in space and zero average of the potential.

In Fig. 6(a), we show the lines in the parameter space that separate the negative $\delta\sigma < 0$, localization-like correction from the positive one $\delta\sigma > 0$. In the presence of strong vector potential disorder $\tau_z \sim \tau_{\rm tr}$, the intravalley interference term is strongly suppressed. This results in the weak-localization sign of the correction even in the case of relatively weak intervalley scattering [see the blue line in Fig. 6(a)]. By contrast, in the presence of relatively weak vector potential disorder $\tau_z^{-1} \ll \tau_{\rm tr}^{-1}$, a substantially stronger intervalley scattering is required to compensate for the intravalley term in (9) and for the correction to have the localization sign.[51] We emphasize that these analytical considerations are entirely restricted to the perturbative regime $k_F\ell_p \gg 1$ of the quantum interference correction to the conductivity and do not apply to the strong localization regime of metal-insulator transitions.

B. Intervalley scattering

Microscopic origin of the intervalley scattering at intermediate densities therefore deserves a more careful consideration. Electrostatic potential can give rise to a strong intervalley scattering only if its amplitude is larger than the bandwidth, in

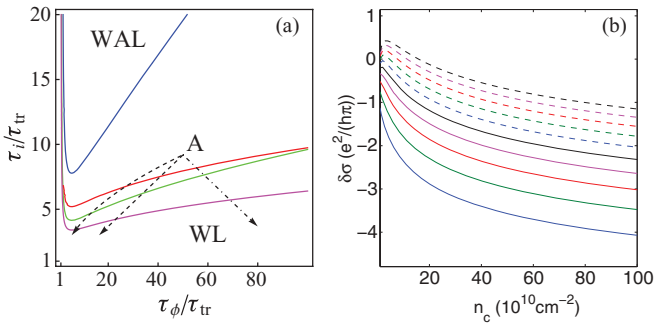

FIG. 6. (Color online) (a) Weak antilocalization to localization crossover boundary in the parameter space of disorder in DLG. Magenta, green, and blue lines correspond to the fixed values of $\tau_\varphi/\tau_z = 100$, 10, and 3, respectively. Red line corresponds to monovalent adsorbate disorder. The dashed lines show example trajectories that a DLG initially at point A takes with changing n_c in case of fixed τ_φ, straight line, and coherence limited by the system size, the curved trajectory $\sim \sqrt{\tau_\varphi/\tau_{\rm tr}}$. Dashed-dotted line corresponds to the trajectory with coherence limited by electron-electron interactions in the diffusive regime [Eq. (13)]. (b) Weak-localization correction for different values $0.1\ \mu{\rm m} \leqslant v_F\tau_i \leqslant 1\ \mu{\rm m}$ from bottom to top with $n_s = 5\times10^{10}\ {\rm cm}^{-2}$. We assume $n_i = 10^{12}\ {\rm cm}^{-2}$ at $z = -20$ nm and dephasing is limited by the electron-electron interactions in the diffusive regime $T\tau \ll 1$ [Eq. (13)]. We took $v_F\tau_\varphi = 0.3\ \mu{\rm m}$ at $n_c = 10^{10}\ {\rm cm}^{-2}$.

which case the lowest-order Born approximation is insufficient (see Appendix and Ref. 52 for details). Such strong potentials can be induced by lattice defects and adsorbate molecules chemically bound to carbon atoms of the graphene lattice. Scattering characteristics of such defects depend strongly on the detailed nature of the electronic structure, type of the chemical bonding, and the position of the defect in the unit cell of graphene.[53] Such details are beyond the scope of the present analysis. Instead, we employ a more generic phenomenological model of two types of scatterers, namely, resonant scatterers and short-range disorder. The former describes the effect of monovalent chemical groups and vacancies in the graphene lattice.[54–56] The scattering rate in this case decreases with density $\tau_R^{-1} \sim (\sqrt{n}\ln n)^{-1}$, which in monolayer graphene is practically indistinguishable from that due to charged defects $1/\tau_{\rm tr}^C \sim 1/\sqrt{n}$ (see Ref. 2). The short-range scatterer model describes atomic defects that do not give rise to resonant scattering. The corresponding scattering amplitude grows with density $\tau^{-1} \sim \sqrt{n}$ and the resulting contribution to the conductivity is density independent. In the case of both sources of intervalley scattering, a relatively weak τ_{iv}^{-1} is sufficient for the quantum correction to have the weak localization sign [Fig. 6(a)].

There exists substantial experimental evidence for the presence of intervalley scattering in graphene. In particular, the observation of negative weak-localization magnetoresistance suggests a rather high intervalley scattering rate corresponding to $L_{iv} \equiv \sqrt{D\tau_{iv}} \sim 0.1$–$0.3\ \mu$m at high densities $n > 10^{11}\ {\rm cm}^{-2}$.[22–31,57] Alternative measurements of a weak D peak in the Raman spectrum demonstrated the presence of intervalley scattering at high energies $\sim$1 eV.[58] More detailed quantitative characteristics of the intervalley scattering such as density dependence are not currently available experimentally.

C. Phase-breaking effect

The size of the self-intersecting trajectories that give rise to the interference correction is limited by either the system size or the phase-breaking effect. The latter can be caused by scattering on magnetic defects[59] or inelastic electron-phonon or electron-electron collisions.[60] Both latter effects result in temperature-dependent dephasing rate τ_φ^{-1}, which is linear $\tau_\varphi^{-1} \sim T$ in the case of electron-phonon scattering and linear or quadratic in the case of electron-electron interactions in the diffusive and ballistic regimes, respectively. Experiments report typical values for the dephasing length $\sqrt{D\tau_\varphi} \sim 2\ \mu$m at the lowest temperatures $T \leqslant 1$ K (Refs. 22–26) and $L_\varphi \sim 0.2\ \mu$m at higher temperatures $T \sim 20$ K. More recent measurements on large-area epitaxial graphene devices accessed very high-temperature regime $T \sim 100$ K corresponding to a short dephasing length $L_\varphi \sim 0.04\ \mu$m.[59,61] The available experimental information about the density, disorder, and temperature-dependent phase-breaking length in graphene is, however, not extensive, and more work is needed before definite quantitative statements can be made in details.

D. Effect of screening on the dephasing rate due to inelastic electron-electron collisions

In this section, we estimate the effect of additional screening on the dephasing rate caused by inelastic electron-electron collisions with low-energy transfer $\hbar\omega \lesssim k_B T$. We estimate the phase-breaking rate up to a numerical coefficient using the self-consistent approach,[34,35,62–64] which is sufficient to analyze the dependence of the phase-breaking rate on the densities in the two layers of DLG. There are two distinct dephasing temperature regimes, diffusive $k_B T \gg \hbar\tau_{\rm tr}^{-1}$ and ballistic $k_B T \ll \hbar\tau_{\rm tr}^{-1}$, which correspond to distinct temperature dependencies of τ_φ^{-1}.

In the diffusive regime $k_B T\tau_{\rm tr} \ll \hbar$, electrons undergo diffusive motion which increases the time they spend in the vicinity of each other (where interaction is the strongest) and therefore enhances the inelastic-scattering rate. Electron-electron collision rate is given by the Fermi golden rule

$$\frac{1}{\tau_{\rm in}} = 4\pi\nu^3 \int_{-\infty}^{\infty} d\omega\, d\epsilon' F(\epsilon,\epsilon',\omega) W^2(\omega),$$
$$F(\epsilon,\epsilon',\omega) = f'_\epsilon(1-f_{\epsilon-\omega})(1-f_{\epsilon'+\omega}) + (1-f'_\epsilon) f_{\epsilon-\omega} f_{\epsilon'+\omega}, \quad (10)$$

where $f_\epsilon \equiv 1/[1+\exp(\beta\epsilon)]$ and $\beta^{-1} = k_B T$. The interaction kernel in (10) is given by

$$W^2(\omega) = \frac{1}{\nu^4} \sum |\langle\alpha\gamma|U_{11}|\beta\delta\rangle|^2 \delta(\epsilon-\epsilon_\alpha)\delta(\epsilon'-\epsilon_\gamma) \times \delta(\epsilon-\omega-\epsilon_\beta)\delta(\epsilon'+\omega-\epsilon_\delta). \quad (11)$$

The matrix element of the screened interaction is written in terms of exact eigenstates $|\alpha\rangle$ of noninteracting Dirac Hamiltonian in the presence of a given disorder potential. The screened electron-electron interaction potential in DLG is given by $U_{11}(q,\omega) = \frac{v_q}{\varepsilon_0(q,\omega)}$ which includes the dynamical dielectric function of Eq. (4) where we need to set $z = 0$ for interaction within the studied layer.

The expression for the collision rate (10) has to be averaged over disorder realizations. The result of this averaging can be then expressed in terms of the diffusion propagator in graphene $D(q,\omega)$, which describes the transport of the charge density through the disordered system. The diffusion propagator is found by solving the diffusion equation $(\partial_t - \Delta D_1)\, D(\mathbf{r},\mathbf{r}') = \delta(\mathbf{r}-\mathbf{r}')$ in the studied layer.[65] Here, D_i is the diffusion coefficient in the studied $(i=1)$ or control $(i=2)$ layer, respectively. As a result, Eq. (10) at $q\ell_1 \ll 1$ and $\omega\tau_{\rm tr} \ll 1$ takes the form

$$\frac{1}{\tau_\varphi} = \frac{8\nu}{\pi} \int_{\tau_\varphi^{-1}} \frac{d\omega\, d^2q}{(2\pi)^2} \frac{\omega|U(q,\omega)|^2}{\sinh\omega} [{\rm Re}D(q,\omega)]^2, \quad (12)$$

where we keep only the logarithmically divergent terms. Also, we introduce a low-energy cutoff $\omega \sim \tau_\varphi^{-1}$ which reflects the fact that only collisions with large enough energy transfer $\omega \gtrsim \tau_\varphi^{-1}$ produce a substantial dephasing of the electrons with diffusion time limited by τ_φ.[34,35,66] Solving (12) self-consistently gives an estimate for the dephasing rate.

At high densities such that $q\ell_i \gg 1, i = 1,2$, the screening is ballistic for which case we can approximate $q v_q \chi_{ii}(q,0) \approx \kappa_i$, and Eq. (12) gives

$$\frac{1}{\tau_\varphi} = \tilde{C} \frac{T}{8\pi\nu_1 D_1} \ln \pi\nu_1 D_1, \quad (13)$$

with

$$\tilde{C} \approx \frac{1}{2} \frac{\zeta^2}{\left(\zeta + \frac{\kappa_2}{\kappa_1}\right)^2}, \quad (14)$$

where we introduce the screening parameter $\kappa_i = 8\pi e^2\nu_i$ for the ith layer and $\zeta \equiv 1 + 2d\kappa_2$.

At lower densities, the polarization operator acquires a diffusion pole

$$\chi_i(q,\omega) \approx g\nu_i \left(1 + i\omega \frac{1}{-i\omega + D_i q^2}\right). \quad (15)$$

The presence of the diffusion pole affects only the coefficient in Eq. (13). In the case of short screening length $\kappa_i = 8\pi e^2\nu_i > \ell_{\rm tr}^{-1}$, we obtain, for the coefficient $C \to \tilde{C}$,

$$C = \frac{1}{1 + \frac{\kappa_2}{\kappa_1}\frac{D_2}{D_1}} \frac{\left(\zeta + \frac{\kappa_2}{\kappa_1}\right) + \frac{D_2}{D_1}\zeta^2\left(1 + \frac{\kappa_2}{\kappa_1}\frac{D_2}{D_1}\right)}{\left(\zeta + \frac{\kappa_2}{\kappa_1}\right)\left(1 + \left(\zeta + 2\frac{\kappa_2}{\kappa_1}\right)\frac{D_2}{D_1}\right)}. \quad (16)$$

In the limit of $\kappa_2/\kappa_1 \gg 1$, the results (16) and (14) both approach

$$C \approx \frac{1}{2}\frac{\kappa_1^2}{\kappa_2^2}. \quad (17)$$

The dephasing rate (13) is strongly dependent on the screening density n_c in the control layer through the diffusion coefficient D_1 and the factor C or $\tilde{C}$.

In the high-temperature $T\tau_{\rm tr} \gg 1$ ballistic regime, the polarization operator is approximated by the free-particle form[40,41] $\chi_i(q,\omega) \approx g\nu_i(1 + i\frac{\omega}{v_F q})$ at $\omega/(v_F q) \ll 1$. The dephasing rate in this case is given by[67]

$$\frac{1}{\tau_\varphi} \approx \frac{(k_B T)^2}{16\nu_1\left(\zeta + \frac{\kappa_2}{\kappa_1}\right)} \ln \frac{k_B T}{16\pi v_F^2 \nu_1}, \quad (18)$$

where parameters $\kappa_i = 8\pi e^2\nu_i$ and $\zeta \equiv 1 + 2d\kappa_2$ have the same meaning as above, and we assume $\kappa_i d \ll 1$.

E. Gate-tunable quantum interference correction

In the presence of mixed scattering sources, the suppression of the transport scattering rate with growing n_c results in the increased relative strength of neutral scattering mechanisms. This is a simple consequence of the Coulomb scattering being effectively screened out by the control layer. As a result, the amplitude of the quantum interference correction varies as a function of n_c. To illustrate this, we assume a large concentration of charged defects n_i located in the SiO_2 substrate and a small concentration of resonant scatterers $\tilde{n}_i$. Then, we have $\tau_{\rm tr}^{-1} \approx \tau_C^{-1} + 2\tau_{iv}^{-1}$ where we use $\tau_z^{-1} \approx \tau_{iv}^{-1}$ valid for a small concentration of single-site defects. In the present analysis, we ignore the effect of screening by the control layer on the shift of the chemical potential in graphene due to charged defects.

Depending on the mechanism limiting the phase coherence, a variety of behaviors of the conductivity correction as a function of the screening density n_c are possible [see Fig. 6(a)]. For screening independent τ_φ^{-1} due to dephasing by magnetic impurities, the system initially at point "A" in Fig. 6(a) takes a trajectory represented by the straight dashed line. In smaller devices, coherence is more likely to be limited by the system size, in which case the effective rate $\tau_\varphi^{-1} \equiv \frac{D}{L^2} = \frac{v_F \ell_{\rm tr}}{2L^2}$ depends on the diffusion coefficient and hence is sensitive to the screening effect of the control layer. This regime corresponds to the curved dashed trajectory in Fig. 6(a). The effect of screening by the control layer is the strongest in the case of dephasing limited by electron-electron interactions. In this case, the ratio $\tau_\varphi/\tau_{\rm tr}$ depends on n_c through the coefficient C in Eq. (13), and the system takes the trajectory shown as the dashed-dotted line in Fig. 6(a). This is the situation most likely to be realized in experiments on large exfoliated flakes of graphene. Dependence of the weak-localization correction on n_c for this case is given by Eq. (9) combined with (5) and (16), which is shown in Fig. 6(b). The effect of additional screening by control layer therefore expands the parameter range in which the weak-localization sign of the quantum correction could be observed, and thus the possibility of a transition from the weak antilocalization to weak localization as a function of the control layer density (i.e., gate tunable) in the nominally metallic studied layer is very high in this case. This predicted transition has not yet been seen in experiments, but may actually exist in the samples of Ref. 9 in the metallic regime of the studied layer.

Weak-field magnetoresistance allows an unambiguous measurement of the weak-localization correction. At small fields $B \ll B_\varphi = h/e(D\tau_\varphi)$, the magnetoresistance can be approximated by

$$\delta\sigma \approx \frac{e^2}{24\pi h}\left(\frac{B}{B_\varphi}\right)^2 \Phi\left(\frac{\tau_\varphi}{\tau_{iv}}, \frac{\tau_\varphi}{\tau_z}\right),$$
$$\Phi\left(\frac{\tau_\varphi}{\tau_{iv}}, \frac{\tau_\varphi}{\tau_z}\right) \equiv \left[1 - \frac{1}{\left(1+2\frac{\tau_\varphi}{\tau_{iv}}\right)^2} - \frac{2}{\left(1+\frac{\tau_\varphi}{\tau_{iv}}+\frac{\tau_\varphi}{\tau_z}\right)^2}\right]. \quad (19)$$

In this regime, we expect a gate-tunable crossover from weak-antilocalization to weak-localization magnetoresistance to be observable especially at higher temperatures.

V. COMPARISON WITH EXPERIMENT

In this section, we discuss the relation of the theory presented above to the recent transport measurements in DLG.[9] The clever DLG design of Ref. 9 provides an opportunity to use the additional gate tunability of the resistivity in the studied layer

$$\rho(n_s,n_c) = \rho_C(n_s,n_c) + \rho_R(n_c) \quad (20)$$

to distinguish the contributions of charged $\rho_C(n_s,n_c)$ and neutral $\rho_R(n_c)$ scattering mechanisms in the intermediate density regime (see Sec. III D). The latter can be deduced from the dependence of the mobility of the studied layer $\mu(n_c)$ on the control layer density reported in the Supplemental Material of Ref. 9. On the one hand, these data are consistent with the presence of a high concentration of charged defects $n_i \approx 10^{12}$ cm^{-2} at the surface of SiO_2 substrate located at $z = -20$ nm away from the studied layer.[9] On the other hand, a similar behavior could result from a smaller concentration of charged defects $n_i \approx 10^{11}$ cm^{-2} in close vicinity of the studied layer or on top of the control layer [see Fig. 5(b) for comparison]. The two situations may be distinguished experimentally by comparing the transport and momentum relaxation rates [see Fig. 4(b)]. At low carrier densities, however, the precise location of impurities does not play an important role and therefore the substantially larger concentration of defects likely to be present in SiO_2 dominates the transport properties.

The situation is different in the case of density inhomogeneity. We find that DLG is relatively inefficient in screening out electron-hole puddles induced by the high concentration of defects in SiO_2 as well as defects in close proximity to the studied graphene layer itself. Both allow some control in the experiments: the former can be reduced by changing the substrate, and the latter may be reduced by improving the sample preparation. Moreover, both improvements were recently implemented in suspended devices.[13]

In the absence of more systematic data, we can estimate the residual mobility associated with neutral scattering mechanisms from the maximum of the mobility curve $\mu(n_c)$ at the maximum density in control layer reported in the Supplemental Material of Ref. 9. The result is $\mu(n_s = 10^{11}) \sim 1.2 \times 10^5$ cm^{-2} V^{-1} s^{-2}, which corresponds to a relatively small density of resonant scatterers, such that $v_F\tau_R \gtrsim 0.8$ μm suggesting that the DLGs analyzed in Ref. 9 may demonstrate gate-tunable weak antilocalization to localization crossover at intermediate densities.

Finally, we discuss the effect of coupling between graphene and hBN substrate which gives rise to spectacular new features in the electron spectrum at high densities.[68] However, at low carrier densities, this effect is not expected to be dramatic. Transport characteristics of graphene could be affected in three possible ways: (i) triangular symmetry of hBN breaks the sublattice symmetry of graphene and therefore gives rise to an additional trigonal warping of the Fermi surface;[69] our estimate shows negligible effect on the weak-localization correction at low densities $n_s \lesssim 10^{11}$ cm^{-2}; (ii) hBN-induced Moire pattern may dominate the density fluctuation at the neutrality point. This effect, however, has not been clearly identified in the local probe data[4] to this point and therefore we expect it to be smaller than current levels of inhomogeneity induced by charged

defects; (iii) additional intervalley scattering may be caused by strong coupling of graphene to hBN. However, existing experimental data and *ab initio* calculations[70] suggest a rather weak coupling which is not expected to give rise to strong intervalley scattering. Nevertheless, a more detailed analysis is required to completely rule out all of these possibilities.

VI. DISCUSSION AND CONCLUSION

Our goal in this work has been a careful theoretical study of the screening by the control layer in determining transport properties of the studied layer in double-layer graphene systems experimentally introduced in Ref. 9. The problem of interest to us is both subtle and complex, involving many disparate aspects of electronic transport phenomena, and our study is at best an approximate one because of the highly complex nature of the problem. In particular, we are interested in studying both semiclassical Boltzmann and quantum localization contributions to the DLG resistivity, including the control layer screening effect, on an equal footing as much as possible. Since potential intravalley and intervalley elastic scattering affect quantum localization properties qualitatively differently, our work must include all mechanisms in the presence of control layer screening with equivalent considerations for all scattering processes contributing to the semiclassical and the quantum parts of graphene resistivity. Since the phase-breaking length arising from inelastic scattering processes is an important ingredient in determining localization effects arising from quantum interference, we consider electron-electron interaction induced inelastic phase decoherence effects in our theory, neglecting electron-phonon interaction which is known to be weak in graphene.[71] We also neglect all direct contributions to transport from inelastic scattering processes since our interest is relatively low-temperature transport where quantum interference may play a role rather than high-temperature transport where inelastic phonon scattering plays a role. We investigate the role of the control layer screening on the density inhomogeneity (i.e., electron-hole puddles) near the Dirac point, finding that screening by the control layer is ineffective in suppressing the electron-hole puddles arising from charged impurities in the SiO_2 substrate far from the studied graphene layer (in fact, this is an important qualitative result of our work). Finally, our work treats both long-range Coulomb disorder arising from random charged impurities in the environment and the short-range disorder arising from neutral atomic defects on an equal footing.

Since the theory involves (at least) six different independent characteristic length scales (elastic mean-free path due to long- and short-range disorder and intravalley and intervalley scattering lengths, the inelastic phase-breaking length, the Fermi wavelength, the density fluctuation correlation length, the thermal length, etc.), it is necessarily a complex problem necessitating various approximations focusing on different aspects of the transport phenomena. We concentrate on low-temperature transport at relatively high "metallic" densities where the quantum interference contribution to the resistivity can be treated as a perturbative weak-localization correction to the semiclassical Boltzmann resistivity. This precludes us from commenting directly on the very low-density nonperturbative insulating behavior (as observed in Ref. 9) from the perspective of strong Anderson localization phenomenon, but our theory establishes the clear possibility of a gate-tunable transition from weak-antilocalization to weak-localization behavior in graphene at metallic densities, which would be a necessary precursor to a possible strong localization crossover behavior at low densities. Whether such a weak-localization transition, which must precede any strong-localization-induced low-density metal-insulator transition, is operational in Ref. 9 was unfortunately not studied there, and the prediction of such a gate-tunable transition in the weak-localization behavior is an important prediction of our work. We emphasize that such transition must be studied at relatively low temperatures, and it may be missed at the higher-temperature range (10–100 K) of study used in Ref. 9. In addition, the strong-localization-induced insulating behavior at low carrier density should be exponential in temperature, and not a power law as observed in Ref. 9. Given our concrete theoretical predictions, we hope that future experiments on DLG systems will resolve the important question of a possible low-density quantum localization transition in clean graphene. Our work shows that it is possible for the intervalley scattering in graphene to be strong enough to induce localization, but at the same time be weak enough not to strongly suppress high-density mobility, particularly in the presence of screening by the control layer.

In conclusion, we analyze the effect of gate-tunable screening provided by the additional control layer in DLG on both classical and quantum parts of the resistivity of a high-quality studied layer in which elastic scattering is limited by charged disorder. We find the following: (i) The additional screening in DLG is relatively inefficient at screening out electron-hole puddles induced by the high concentration of defects in SiO_2 as well as defects in close proximity to the studied graphene layer itself. In the latter cases, the screening provides roughly a factor of 2 suppression within the control layer density range of 10^{10}–10^{12} cm^{-2}. Therefore, the suppression of electron-hole puddles itself is insufficient to explain the contrast between the strongly insulating behavior observed in DLG (Ref. 9) structures and the absence of such in stand-alone graphene samples including highly homogeneous suspended samples.[13] (ii) The screening effect of control layer results in a relatively strong suppression of the elastic relaxation rate resulting in gate-tunable mobility of the studied layer in the DLG at intermediate density n_s. (iii) We show that the location of the charged defects limiting the mobility of the DLG can be determined by measuring the ratio of the momentum relaxation and transport relaxation rates. (iv) Additional screening effect of the control layer strongly suppresses the potential of Coulomb interaction between charge carriers. (v) The combined effect of (ii) and (iv) results in a strong suppression of the dephasing rate due to inelastic electron-electron collisions which determines the sign and the magnitude of the quantum interference correction to the resistivity. (vi) As a consequence of (ii) and (v), the weak-localization correction to the resistivity is gate tunable. (vii) The very low concentration of resonant or short-range scatterers that has little effect on the Boltzmann part of the resistivity in the high-quality studied layer in DLG nevertheless can provide sufficient intervalley scattering for the quantum correction to resistivity to have a negative (weak-localization) sign. Moreover, the additional screening in DLG improves the coherence in the

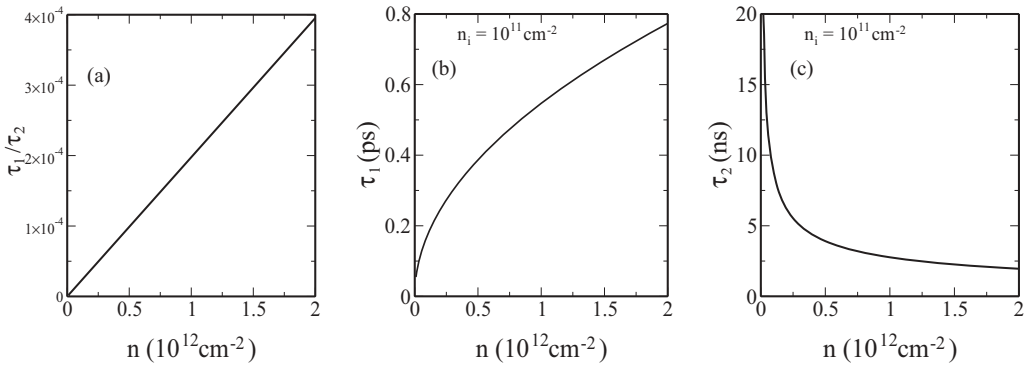

FIG. 7. The ratio of intravalley scattering time (τ_1) to intervalley scattering time (τ_2), τ_1/τ_2, or equivalently, the ratio of the scattering rates γ_2/γ_1, where $\gamma_i = \hbar/\tau_i$ for the long-range Coulomb potential. (b) and (c) show τ_1 and τ_2, respectively, as a function of density for an impurity density $n_i = 10^{11}$ cm^{-2}. Note that $\tau_1 \propto n^{1/2}$ and $\tau_2 \propto n^{-1/2}$.

system and therefore expands the range in which quantum correction of weak-localization sign is observable. (viii) We find that high-quality DLG structures where charged defects are the dominant source of elastic scattering manifest a peculiar gate-tunable crossover between weak-antilocalization and weak-localization magnetoresistance. The latter could be observed in the intermediate density regime in which electron density in the studied layer is sufficiently high for random inhomogeneity to be neglected and the transport to be metallic and at the same time is low enough for the effect of the control layer screening to be substantial (see also Sec. III D).

In this paper, we developed a theoretical framework that can be used for a systematic experimental characterization of the symmetry-breaking mechanisms in DLG in the intermediate density regime which could allow further understanding of the observed strongly insulating behavior at low densities. This work could also be used to describe a more generic double-layer heterostructure involving materials other than graphene that realize other universality classes of Dirac electrons such as surfaces of strong and weak topological insulators. Such heterostructures could be useful to study experimentally gate-tunable quantum interference and Anderson localization effects in these systems, which are a topic of active current theoretical interest.[72]

ACKNOWLEDGMENT

This work is supported by US-ONR-MURI and NRI-SWAN.

APPENDIX: INTERVALLEY SCATTERING DUE TO CHARGED DEFECTS

The intervalley scattering rate due to Coulomb impurities can be separated from the intravalley part by taking low- and high-momentum parts of the sum over $\mathbf{p}' = \mathbf{p} + \mathbf{q} + \mathbf{G}$ in Eq. (5), where $\mathbf{G}$ is the reciprocal lattice vector. For intravalley scattering, we include only $\mathbf{G} = 0$ which results in

$$\frac{1}{\tau_1^C} = \frac{n_i \nu}{\hbar} \int_0^{2k_F} \frac{q^2 dq}{k_F^3} \left[\frac{V(q)}{\epsilon(q)}\right]^2 \sqrt{1-(q/2k_F)^2}. \quad \text{(A1)}$$

For intervalley scattering, we take the smallest allowed reciprocal vector that connects the two corners of the hexagonal Brillouin zone $|\mathbf{G}| = |\mathbf{K} - \mathbf{K}'| = 2\pi/3a$, where $a = 1.42$ Å is the C-C distance. Then, the intervalley scattering time is given by

$$\frac{1}{\tau_2^C} = \frac{n_i \nu}{\hbar} \frac{1}{k|\mathbf{G}-\mathbf{k}|} \int_{q_-}^{q_+} q\, dq [V(q)]^2 \sin\theta, \quad \text{(A2)}$$

where $q_\pm = |\mathbf{G} - \mathbf{p}| \pm p$ and $\sin\theta$ is given by the following relation:

$$q = \sqrt{|\mathbf{G}-\mathbf{p}|^2 + p^2 - 2|\mathbf{G}-\mathbf{p}| p \cos\theta}. \quad \text{(A3)}$$

In Fig. 7, we show the calculated ratio of intravalley scattering time to intervalley scattering time τ_1^C/τ_2^C as a function of density for the long-range Coulomb impurities. Since the ratio is very small, the intervalley scattering plays a little role in the transport when the Coulomb disorder dominates. At the same time, a phenomenological model of delta-range disorder gives $\tau_1/\tau_2 = 1$ at all densities.

[1] S. Adam, E. H. Hwang, V. M. Galitski, and S. Das Sarma, Proc. Natl. Acad. Sci. USA **104**, 18392 (2007).
[2] S. Das Sarma, S. Adam, E. H. Hwang, and E. Rossi, Rev. Mod. Phys. **83**, 407 (2011).
[3] J. Martin, N. Akerman, G. Ulbricht, T. Lohmann, J. H. Smet, K. von Klitzing, and A. Yacoby, Nat. Phys. **4**, 144 (2008).
[4] J. Xue, J. Sanchez-Yamagishi, D. Bulmash, P. Jacquod, A. Deshpande, K. Watanabe, T. Taniguchi, P. Jarillo-Herrero, and B. J. LeRoy, Nat. Mater. **10**, 282 (2011).
[5] R. Decker, Y. Wang, V. W. Brar, W. Regan, H.-Z. Tsai, Q. Wu, W. Gannett, A. Zettl, and M. F. Crommie, Nano Lett. **11**, 2291 (2011).
[6] P. Cao, J. O. Varghese, K. Xu, and J. R. Heath, Nano Lett. **12**, 1459 (2012).
[7] K. S. Novoselov, A. K. Geim, S. V. Morozov, D. Jiang, M. I. Katsnelson, I. V. Grigorieva, S. V. Dubonos, and A. A. Firsov, Nature (London) **438**, 197 (2005).

[8] M. Z. Hasan and C. L. Kane, Rev. Mod. Phys. **82**, 3045 (2010); X.-L. Qi and S.-C. Zhang, *ibid.* **83**, 1057 (2011); S. Adam, E. H. Hwang, and S. Das Sarma, Phys. Rev. B **85**, 235413 (2012).

[9] L. A. Ponomarenko, A. K. Geim, A. A. Zhukov, R. Jalil, S. V. Morozov, K. S. Novoselov, I. V. Grigorieva, E. H. Hill, V. V. Cheianov, V. I. Falko, K. Watanabe, T. Taniguchi, and R. V. Gorbachev, Nat. Phys. **7**, 958 (2011).

[10] S. Das Sarma, E. H. Hwang, and Q. Li, Phys. Rev. B **85**, 195451 (2012).

[11] I. L. Aleiner and K. B. Efetov, Phys. Rev. Lett. **97**, 236801 (2006); A. Altland, *ibid.* **97**, 236802 (2006); P. M. Ostrovsky, I. V. Gornyi, and A. D. Mirlin, *ibid.* **98**, 256801 (2007); Eur. Phys. J.: Special Topics **148**, 63 (2007).

[12] Kentaro Nomura and A. H. MacDonald, Phys. Rev. Lett. **98**, 076602 (2007); J. H. Bardarson, J. Tworzydło, P. W. Brouwer, and C. W. Beenakker, *ibid.* **99**, 106801 (2007); Kentaro Nomura, Mikito Koshino, and Shinsei Ryu, *ibid.* **99**, 146806 (2007); Shi-Jie Xiong and Ye Xiong, Phys. Rev. B **76**, 214204 (2007); C. H. Lewenkopf, E. R. Mucciolo, and A. H. Castro Neto, *ibid.* **77**, 081410(R) (2008); Aurélien Lherbier, Blanca Biel, Yann-Michel Niquet, and Stephan Roche, Phys. Rev. Lett. **100**, 036803 (2008); N. Leconte, A. Lherbier, F. Varchon, P. Ordejon, S. Roche, and J.-C. Charlier, Phys. Rev. B **84**, 235420 (2011).

[13] A. S. Mayorov, D. C. Elias, I. S. Mukhin, S. V. Morozov, L. A. Ponomarenko, K. S. Novoselov, A. K. Geim, and R. V. Gorbachev, Nano Lett. **12**, 4629 (2012).

[14] F. Amet, J. R. Williams, K. Watanabe, T. Taniguchi, D. Goldhaber-Gordon, arXiv:1209.6364.

[15] Y.-W. Tan, Y. Zhang, H. L. Stormer, and P. Kim, Eur. Phys. J.: Special Topics **148**, 15 (2007).

[16] J. Heo, H. J. Chung, S.-H. Lee, H. Yang, D. H. Seo, J. K. Shin, U.-In. Chung, S. Seo, E. H. Hwang, and S. Das Sarma, Phys. Rev. B **84**, 035421 (2011).

[17] K. I. Bolotin, K. J. Sikes, J. Hone, H. L. Stormer, and P. Kim, Phys. Rev. Lett. **101**, 096802 (2008); X. Du, I. Skachko, A. Barker, and E. Y. Andrei, Nat. Nanotechnol. **491**, 491 (2008).

[18] E. H. Hwang and S. Das Sarma, Phys. Rev. B **79**, 165404 (2009).

[19] Q. Li, E. H. Hwang, and S. Das Sarma, Phys. Rev. B **84**, 115442 (2011).

[20] E. H. Hwang and S. Das Sarma, Phys. Rev. B **77**, 195412 (2008).

[21] X. Hong, K. Zou, and J. Zhu, Phys. Rev. B **80**, 241415 (2009).

[22] Y.-F. Chen, M.-H. Bae, C. Chialvo, T. Dirks, A. Bezryadin, and N. Mason, J. Phys.: Condens. Matter **22**, 205301 (2010).

[23] F. V. Tikhonenko, D. W. Horsell, R. V. Gorbachev, and A. K. Savchenko, Phys. Rev. Lett. **100**, 056802 (2008).

[24] D.-K. Ki, D. Jeong, J.-H. Choi, H.-J. Lee, and K.-S. Park, Phys. Rev. B **78**, 125409 (2008).

[25] J. Berezovsky and R. M. Westervelt, Nanotechnology **21**, 274014 (2010).

[26] F. V. Tikhonenko, A. A. Kozikov, A. K. Savchenko, and R. V. Gorbachev, Phys. Rev. Lett. **103**, 226801 (2009).

[27] B. Jouault, B. Jabakhanji, N. Camara, W. Desrat, C. Consejo, and J. Camassel, Phys. Rev. B **83**, 195417 (2011).

[28] W. Pan, A. J. Rose, III, S. W. Howell, T. Ohta, T. A. Friedmann, and C.-T. Liang, New J. Phys. **13**, 113005 (2011).

[29] M. Woszczyna, M. Friedemann, K. Pierz, T. Weimann, and F. J. Ahlers, J. Appl. Phys. **110**, 043712 (2011).

[30] X. Wu, X. Li, Z. Song, C. Berger, and W. A. de Heer, Phys. Rev. Lett. **98**, 136801 (2007).

[31] Y. Oh, J. Eom, H. C. Koo, and S. H. Han, Solid State Commun. **150**, 1987 (2010).

[32] E. McCann, K. Kechedzhi, V. I. Fal'ko, H. Suzuura, T. Ando, and B. L. Altshuler, Phys. Rev. Lett. **97**, 146805 (2006).

[33] H. Suzuura and T. Ando, Phys. Rev. Lett. **89**, 266603 (2002); D. V. Khveshchenko, *ibid.* **97**, 036802 (2006); A. F. Morpurgo and F. Guinea, *ibid.* **97**, 196804 (2006).

[34] B. Altshuler and A. Aronov, *Electron-Electron Interactions in Disordered Systems* (Elsevier, Amsterdam, 1985).

[35] E. Akkermans and G. Montambaux, *Mesoscopic Physics of Electrons and Photons* (Cambridge University Press, New York, 2007).

[36] G. D. Mahan, *Many-Particle Physics*, 3rd ed. (Kluwer Academic, New York, 2000).

[37] Coulomb interaction for graphene encapsulated in hexagonal boron nitride is characterized by a dimensionless constant $e^2/(\Xi\hbar v_F) \approx 0.4$, where we took the dielectric constant to be $\Xi \approx 5$.

[38] S. Das Sarma and A. Madhukar, Phys. Rev. B **23**, 805 (1981).

[39] Kenneth W.-K. Shung, Phys. Rev. B **34**, 979 (1986).

[40] B. Wunsch, T. Stauber, F. Sols, and F. Guinea, New J. Phys. **8**, 318 (2006).

[41] E. H. Hwang and S. Das Sarma, Phys. Rev. B **75**, 205418 (2007).

[42] V. M. Galitski, S. Adam, and S. Das Sarma, Phys. Rev. B **76**, 245405 (2007).

[43] S. Adam, E. Hwang, E. Rossi, and S. D. Sarma, Solid State Commun. **149**, 1072 (2009); E. Rossi and S. Das Sarma, Phys. Rev. Lett. **101**, 166803 (2008); E. Rossi, S. Adam, and S. Das Sarma, Phys. Rev. B **79**, 245423 (2009).

[44] S. Das Sarma and E. H. Hwang, Phys. Rev. B **83**, 121405 (2011).

[45] V. V. Cheianov, V. I. Fal'ko, B. L. Altshuler, and I. L. Aleiner, Phys. Rev. Lett. **99**, 176801 (2007).

[46] D. Bruggeman, Ann. Phys. (NY) **416**, 636 (1935); M. Hori and F. Yonezawa, J. Math. Phys. **16**, 352 (1975).

[47] E. Rossi, J. H. Bardarson, M. S. Fuhrer, and S. Das Sarma, Phys. Rev. Lett. **109**, 096801 (2012).

[48] P. M. Ostrovsky, I. V. Gornyi, and A. D. Mirlin, Phys. Rev. B **74**, 235443 (2006).

[49] K. Kechedzhi, E. McCann, V. I. Fal'ko, H. Suzuura, T. Ando, and B. L. Altshuler, Eur. Phys. J.: Special Topics **148**, 39 (2007).

[50] G. Bergmann, Phys. Rep. **107**, 1 (1984).

[51] Corrugations of the graphene sheet give rise to an effective vector potential disorder and therefore increase τ_z^{-1}. This effect is expected to be small in devices used in Ref. 9 since surface roughness of hBN substrate is an order of magnitude smaller than of SiO_2.

[52] Y.-Y. Zhang, J. Hu, B. A. Bernevig, X. R. Wang, X. C. Xie, and W. M. Liu, Phys. Rev. Lett. **102**, 106401 (2009).

[53] T. O. Wehling, S. Yuan, A. I. Lichtenstein, A. K. Geim, and M. I. Katsnelson, Phys. Rev. Lett. **105**, 056802 (2010).

[54] D. M. Basko, Phys. Rev. B **78**, 115432 (2008).

[55] J. P. Robinson, H. Schomerus, L. Oroszlány, and V. I. Fal'ko, Phys. Rev. Lett. **101**, 196803 (2008).

[56] M. Titov, P. M. Ostrovsky, I. V. Gornyi, A. Schuessler, and A. D. Mirlin, Phys. Rev. Lett. **104**, 076802 (2010); P. M. Ostrovsky, M. Titov, S. Bera, I. V. Gornyi, and A. D. Mirlin, *ibid.* **105**, 266803 (2010).

[57] A. Nath Pal, V. Kochat, and A. Ghosh, arXiv:1206.3866 [accepted to Phys. Rev. Lett.].

[58]Z. H. Ni, L. A. Ponomarenko, R. R. Nair, R. Yang, S. Anissimova, I. V. Grigorieva, F. Schedin, P. Blake, Z. X. Shen, E. H. Hill, K. S. Novoselov, and A. K. Geim, Nano Lett. **10**, 3868 (2010).

[59]S. Lara-Avila, A. Tzalenchuk, S. Kubatkin, R. Yakimova, T. J. B. M. Janssen, K. Cedergren, T. Bergsten, and V. Fal'ko, Phys. Rev. Lett. **107**, 166602 (2011).

[60]A. A. Kozikov, A. K. Savchenko, B. N. Narozhny, and A. V. Shytov, Phys. Rev. B **82**, 075424 (2010).

[61]J. Jobst, D. Waldmann, I. V. Gornyi, A. D. Mirlin, and H. B. Weber, Phys. Rev. Lett. **108**, 106601 (2012).

[62]I. L. Aleiner, B. L. Altshuler, and M. E. Gershenson, Waves Random Media **9**, 201 (1999).

[63]B. N. Narozhny, G. Zala, and I. L. Aleiner, Phys. Rev. B **65**, 180202 (2002).

[64]M. Schuett, P. M. Ostrovsky, I. V. Gornyi, and A. D. Mirlin, Phys. Rev. B **83**, 155441 (2011).

[65]K. Kechedzhi, O. Kashuba, and V. I. Fal'ko, Phys. Rev. B **77**, 193403 (2008).

[66]B. L. Altshuler, A. G. Aronov, and D. E. Khmelnitsky, J. Phys. C: Solid State Phys. **15**, 7367 (1982).

[67]Q. Li (unpublished).

[68]M. Yankowitz, J. Xue, D. Cormode, J. Sanchez-Yamagishi, K. Watanabe, T. Taniguchi, P. Jarillo-Herrero, P. Jacquod, and B. J. LeRoy, Nature (London) **8**, 382 (2012).

[69]C. Ortix, L. Yang, and J. van den Brink, Phys. Rev. B **86**, 081405(R) (2012).

[70]B. Sachs, T. O. Wehling, M. I. Katsnelson, and A. I. Lichtenstein, Phys. Rev. B **84**, 195414 (2011).

[71]E. H. Hwang and S. Das Sarma, Phys. Rev. B **77**, 115449 (2008).

[72]S. Ryu, C. Mudry, A. W. W. Ludwig, and A. Furusaki, Phys. Rev. B **85**, 235115 (2012); R. S. K. Mong, J. H. Bardarson, and J. E. Moore, Phys. Rev. Lett. **108**, 076804 (2012); Z. Ringel, Y. E. Kraus, and A. Stern, Phys. Rev. B **86**, 045102 (2012).